Sound absorption of a micro-perforated panel backed by an irregular-shaped cavity

Chunqi Wang[a)] and Li Cheng[b)]
Department of Mechanical Engineering, The Hong Kong Polytechnic University, Kowloon, Hong Kong

Jie Pan
School of Mechanical Engineering, The University of Western Australia, 35 Stirling Highway, Crawley, Western Australia 6009, Australia

Ganghua Yu
Department of Mechanical Engineering, The Hong Kong Polytechnic University, Kowloon, Hong Kong

In the pursuit of more effective noise control devices, the cavity backed micro-perforated panel absorber (CBMPPA) is developed in this study. A CBMPPA differs from the conventional micro-perforated panel (MPP) absorber in that the MPP is backed by a trapezoidal cavity, which allows more effective vibroacoustic coupling between the MPP and the cavity. A two-dimensional theoretical model is established and tested both numerically and experimentally. Based on the verified theoretical model, sound absorption performance of a trapezoidal CBMPPA is investigated numerically. Results show that the shape of the backing cavity can significantly alter the sound absorption mechanisms and frequency distribution of overall sound absorption coefficient of the absorber. Further analyses show that acoustic modes that are initially decoupled from the MPP in the rectangular configuration are coupled with the air motion in the MPP, which accounts for the change in absorption pattern of the trapezoidal CBMPPA. By the same token, it also provides the flexibility for tuning the effective absorption range of the absorber. Due to the varying impedance matching conditions, the absorption performance of the trapezoidal CBMPPA exhibits obvious local characteristics over the MPP surface, which contrasts with the spatially uniform absorption in the conventional MPP absorber. © *2010 Acoustical Society of America.* [DOI: 10.1121/1.3257590]

I. INTRODUCTION

Micro-perforated panel (MPP) has been used as an alternative to traditional porous sound absorbing materials for a number of years. A MPP consists of a sheet panel with a lattice of sub-millimeter size perforations distributed over its surface. By reducing the sizes to sub-millimeter scale, the perforations themselves provide acoustic resistance and low acoustic mass reactance necessary for an absorber without the use of any porous material (Maa, 1975, 1987). As a clean and efficient sound absorbing material, MPP is finding more and more applications in areas such as room acoustics (Fuchs and Zha, 1997; Kang and Fuchs, 1999; Droltleff and Zhou, 2001; Kang and Brocklesby; 2005), environmental noise abatement (Asdrubali and Pispola, 2007), and duct noise control (Wu, 1997). Conventionally, a typical MPP absorber takes the form of a MPP fitted in front of a backing wall, as illustrated in Fig. 1(a). The backing wall is parallel to the MPP with an air gap between them. The air gap provides an acoustic-stiffness, which is controlled by its depth. Together with the perforation, resonance-type absorption is generated. In all the existing work mentioned above, the depth of the air

gap between the MPP and the backing wall is assumed to be a constant value. Previous studies on the MPP absorber mainly focus on the properties of the MPP itself, e.g., orifice diameter, perforation rate, panel thickness and materials, etc. Little attention is paid to the cavity depth as it is usually assumed to be a constant according to the target resonance frequency of the absorber (Maa, 1987).

This work aims to study the sound absorption characteristics of an irregular-shaped cavity backed micro-perforated panel absorber (CBMPPA) with varying cavity depths (a MPP backed by a trapezoidal cavity), as shown in Fig. 1(b). The motivation for changing the constant cavity depth in the conventional MPP absorbers to a varying value is explained as below. From the vibroacoustic viewpoint, the sound absorption of the MPP absorber is dominated by the resonance of the air mass vibration of both the perforated holes and the backing cavity (or the air gap), and the absorption efficiency is limited to the resonance frequency region. Forming a closed space behind the MPP, multi-modal acoustic resonances can be created. For MPP absorbers with rectangular-shaped cavities, however, only a few selected acoustic modes play a role in the sound absorption due to the perpendicular relationship among their three adjacent walls. Other modes, although abundant in number, are decoupled from the air motion inside the micro-perforations of the MPP and hence have no contribution toward the sound absorption. This selective coupling pattern can be altered by setting the MPP

[a)] Present address: Department of Mechanical Engineering, The University of Hong Kong, Pokfulam Road, Hong Kong.
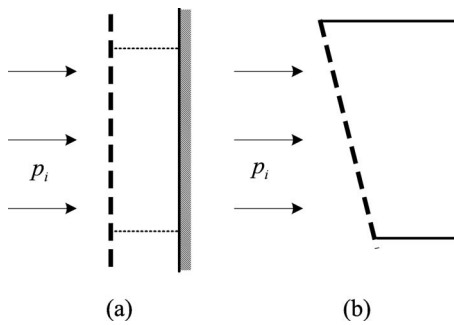[b)] Author to whom correspondence should be addressed. Electronic mail: mmlcheng@inet.polyu.edu.hk

FIG. 1. Schematic of the MPP absorbers. (a) Conventional configuration in which a MPP is backed by a rigid wall or a rigid rectangular cavity (as illustrated by the dotted lines). (b) Irregular-shaped configuration in which a MPP is backed by a rigid trapezoidal cavity.
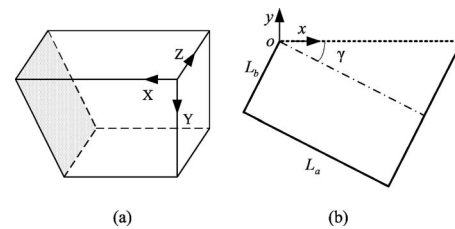

FIG. 2. Theoretical model of the irregular-shaped CBMPPA. (a) The three-dimensional configuration. The inclined wall is covered by a MPP while the other five walls of the trapezoidal cavity are acoustically rigid. (b) The two-dimensional theoretical model.

inclined to the back wall to form a so-called irregular-shaped cavity as opposed to the rectangular one. Previous work showed that the coupling between a structure and an enclosure can be greatly enhanced due to the inclination of the cavity wall (Li and Cheng, 2004; Sum and Pan, 2006). In the present case, acoustic modes that are initially decoupled from the MPP in the rectangular configuration can also be coupled with the air motion in the MPP. The expected result of the increased vibroacoustic coupling is the enhanced sound absorption performance over a wider bandwidth.

The idea of developing the irregular-shaped CBMPPA is also motivated by the practical need in the pursuit of more efficient noise barriers for environmental noise control. Noise barrier design and performance have been well documented in literature (Bies and Hansen, 1996). Since the present study does not claim any contribution in this regard, a literature review on noise barrier simulation and design is omitted here. Despite the significant progress made in the past, measurements have shown that performance of sound barriers is much less than that predicted by theory, especially for parallel barriers and barriers installed in front of noise sources with large reflective surfaces (Fuchs, 2001; Watts, 1996). This phenomenon is attributed to the multiple reflection and over-the-top scattering of the sound waves. To tackle the problem, an innovative wave tapping barrier was developed by Pan et al. (2004). The wave trapping barrier uses a cavity-backed perforated surface tilled toward the road. The panel is composed of a series of wedges, which can take the shape of a trapezoid or, as a degenerated case, a triangle box. The tilted profile allows noise to be trapped for a better absorption and, by the same token, minimizes the noise escaping from the top.

The success of this promising technology is, however, still limited by a number of factors. The first is the lack of a thorough understanding of the sound absorption mechanism of the trapezoidal CBMPPA. The second is the lack of a suitable design tool to optimize and simplify the development of such devices. Both of them require a reliable theoretical model that can describe the vibroacoustic behavior of the CBMPPA accurately. Most previous studies modeled the MPP absorber as an equivalent electrical circuit. Such a method surely applies to the conventional construction as shown in Maa (1975, 1987), but fails when the cavity depth is varying. The transfer matrix method, described in Lee and

Kwon (2004) and Atalla and Sgard (2007), also assumes a constant cavity depth, which becomes powerless in dealing with the irregular-shaped backing cavity. In studying the sound absorption of a finite flexible MPP backed by an air cavity, Lee et al. (2005) developed a solution procedure based on the modal analysis approach. The theoretical model established in Lee et al. (2005) takes into account the full coupling between the cavity acoustics and the panel vibration. However, as it assumes a rectangular cavity and the exterior acoustic loading on the MPP surface is simplified as a uniformly distributed sound pressure, that model cannot be adopted to investigate the irregular-shaped CBMPPA directly.

In what follows, Sec. II outlines the theoretical formulation for the sound absorption of the irregular-shaped CBMPPA based on a two-dimensional (2D) model. A method of solution is established to solve the fully coupled system among the MPP, the irregular-shaped backing cavity, and the exterior sound field. The absorption performance of an irregular-shaped CBMPPA is investigated numerically in Sec. III. Compared with the rectangular CBMPPA of the same cavity volume, the trapezoidal CBMPPA has a quite different absorption pattern with more spectral peaks. With proper geometrical configuration, the trapezoidal CBMPPA can achieve fairly good absorption performance over a wider continuous bandwidth. In addition, the absorption of the trapezoidal CBMPPA demonstrates obvious local characteristics, which is caused by the distorted acoustic modes of the trapezoidal cavity. In Sec. IV, the theoretical model is validated experimentally.

II. THEORETICAL MODELING

Figure 2(a) shows the three-dimensional (3D) configuration of an irregular-shaped CBMPPA, which consists of a trapezoidal cavity and a MPP covering on the inclined wall. The MPP itself can be either flexible or rigid, but it is assumed to be rigid for simplification in this study. The other five cavity walls are assumed to be acoustically rigid. When an acoustic wave p_i is incident on the MPP, some of the acoustic energy is reflected, and the rest is absorbed by the MPP as well as the sound absorbing materials inside the cavity (if any). As long as the inclined wall is parallel to the Z direction and the incident wave is parallel to the X-Y plane, it is appropriate to simplify the 3D configuration as a 2D theoretical model, as shown in Fig. 2(b). For convenience, a proper rotation is performed so that the MPP is laid out hori-

zontally in Fig. 2(b). The trapezoidal cavity is completely defined by the side length L_a, L_b and the inclination angle γ. The local coordinate system xoy defined in Fig. 2(b) is adopted throughout the following presentation.

The theoretical formulation starts with the analytical treatments on the aerial motion and the acoustic impedance of the micro-perforations. With a sound pressure difference applied between the two sides of the MPP, air mass vibration occurs inside the orifice. As a measure to simplify the theoretical modeling, the discrete air particle velocity over each orifice is averaged across the adjacent unperforated region so that a quasicontinuous particle velocity field $\bar{u}(x)$ is obtained. Such a simplification procedure is valid as long as the distance between orifices R is short enough compared with the acoustic wavelength λ, say, $R < \lambda/4$ (Putra, 2007). The acoustic impedance due to the micro-perforations is also averaged over the whole panel so that the relative (to the characteristic impedance $\rho_0 c$ in air) acoustic impedance of the MPP is found as (Maa, 1998)

$$Z = \frac{32\eta t}{\sigma \rho_0 c d^2} \left[\left(1 + \frac{K^2}{32} \right)^{1/2} + \frac{\sqrt{2}}{32} K \frac{d}{t} \right]$$
$$+ i \cdot \frac{\omega t}{\sigma c} \left[1 + \left(1 + \frac{K^2}{2} \right)^{-1/2} + 0.85 \frac{d}{t} \right], \quad (1)$$

where $\omega = 2\pi f$ is the angular frequency, $K = d\sqrt{\omega \rho_0 / 4\eta}$, d is the orifice diameter, t is the panel thickness, η is the coefficient of viscosity, and σ is the perforation ratio. Equation (1) has been shown to be accurate enough when the sound pressure level is less than 100 dB and the orifices are spaced more than a diameter apart (Maa, 1987, 1998). Thus, for normal incident wave p_i with unit amplitude, the acoustic boundary condition on the inclined MPP can be described as

$$Z \cdot \bar{u}(x) = \frac{1}{\rho_0 c} [p_{\mathrm{cav}} - (2p_i + p_{\mathrm{rad}})], \quad (2)$$

where p_{cav} is the sound pressure inside the backing cavity, $2p_i$ is the blocked pressure, and p_{rad} is the external pressure radiated by the particle velocity field $\bar{u}(x)$. Since both p_{cav} and p_{rad} are due to the radiation of the particle velocity field $\bar{u}(x)$, Eq. (2) describes the coupled behavior between the acoustic field and the air motion in the micro-perforations. A method of solution to this coupled equation is presented in Sec. II A.

A. Method of solution

Following the standard Galerkin procedure (Meirovitch, 2001), the particle velocity over the MPP surface $\bar{u}(x)$ is expanded as a series of sine functions

$$\bar{u}(x) = \sum_{j=1}^{J} u_j \sin(j\pi x/L), \quad (3)$$

where u_j is the complex amplitude and L is the length of the inclined wall. With a proper truncation of the decomposition series, Eq. (3) can represent the averaged particle velocity field $\bar{u}(x)$ accurately except at the boundary edges. As far as the vibroacoustic analysis in this study is concerned, the approximation errors of $\bar{u}(x)$ at the boundary edges (the two

ending points in the 2D model) can be neglected. Substituting Eq. (3) into the coupled Eq. (2), multiplying $2\sin(j\pi x/L)$ to both sides, and integrating over the inclined wall ($0 < x < L$) give

$$Z u_j + \frac{2}{\rho_0 c L} \int_0^L (p_{\mathrm{rad}} - p_{\mathrm{cav}}) \sin(j\pi x/L) dx$$
$$= \frac{4}{\rho_0 c L} \int_0^L p_i \sin(j\pi x/L) dx. \quad (4)$$

The sound pressure inside the cavity due to $\bar{u}(x)$, p_{cav}, can be expressed in terms of acoustic modes of the rigid-walled cavity (Cheng, 2005):

$$p_{\mathrm{cav}}(x,y) = \sum_{m=0}^{M} A_m \psi_m(x,y)$$
$$= -\frac{i\rho_0 c^2 \omega}{V} \sum_{m=0}^{M} \frac{\psi_m(x,y)}{\Lambda_m(\omega^2 - \omega_m^2)} \int_0^L \bar{u}(x')\psi_m(x',0)dx', \quad (5)$$

where $\psi_m(x,y)$ is the mth acoustic mode of the trapezoidal cavity, A_m is the complex amplitude for each cavity mode $\psi_m(x,y)$, V is the cavity volume, ρ_0 is the air density, c is the speed of sound in air, and Λ_m is the normalized factor of the mth cavity mode. The acoustic modes of the trapezoidal cavity are found numerically with the commercially available software COMSOL® Multiphysics. In the conventional MPP absorber backed by a rectangular cavity, the cavity modes can be expressed analytically as

$$\psi_{m,n}(x,y) = \cos\left(\frac{m\pi x}{L_a}\right) \cos\left(\frac{n\pi y}{L_b}\right), \quad (6)$$

where L_a and L_b are the side lengths shown in Fig. 2(b) with $\gamma = 0$. Accordingly, Eq. (5) becomes

$$p_{\mathrm{cav}}(x,y) = \sum_{m,n=0}^{M,N} A_{m,n} \psi_{m,n}(x,y). \quad (7)$$

The absolute value of the complex amplitude A_m in Eq. (5) or $A_{m,n}$ in Eq. (7) measures the contribution of each cavity mode toward the sound field in the cavity. In the following presentation, the acoustic modes of the rectangular cavity will be called RC modes and the modes of the trapezoidal cavity will be called TC modes for brevity.

The external pressure imposing on the MPP includes the blocked pressure $2p_i$ and the external radiation by the micro-perforations p_{rad}. For a large array panel which is composed of a group of MPP absorbers arranged periodically, e.g., the sound barrier developed by Pan et al. (2004), the radiated pressure p_{rad} consists of both self-radiation and mutual radiation from other MPP absorbers. Assuming that the array panel is large enough, an approximate periodic (or rigid) boundary condition may be applied to each single MPP absorber, in which the external radiation by each MPP absorber is confined to a virtual rigid duct with infinite length. Another reason for adopting such treatment is that such a boundary condition conforms to the measurement method for the normal incidence absorption coefficient using impedance

tubes, as detailed in Sec. IV. Thus, given the averaged particle velocity distribution $\bar{u}(x)$, the radiated pressure p_{rad} is found as (Doak, 1973)

$$p_{\mathrm{rad}} = \frac{\rho_0}{L} \sum_{n=0}^{\infty} c_n \varphi_n(x) \int_0^L \varphi_n(x') \bar{u}(x') dx', \tag{8}$$

which simulates the situation when the MPP absorber is fixed to one end of a standing wave tube to measure its sound absorption characteristics. In Eq. (8), $\varphi_n(x)$ is the duct acoustics modes of a 2D channel of width L,

$$\varphi_n(x) = \sqrt{2 - \delta_{0n}} \cos(n\pi x/L), \tag{9}$$

where δ_{0n} is the Kronecker delta and c_n is the modal phase speed,

$$c_n = \frac{ic}{\sqrt{(n\pi c/\omega L)^2 - 1}}, \quad n = 1, 2, 3, \ldots. \tag{10}$$

In order to solve Eq. (4), both p_{cav} and p_{rad} are related to the complex amplitudes of the sine series u_j via a modal impedance matrix. Denote the cavity pressure caused by $\sin(j\pi x/L)$ as $p_{\mathrm{cav},j}$, that is,

$$p_{\mathrm{cav},j} = -\frac{i\rho_0 c^2 \omega}{V} \sum_{m=0}^{M} \frac{\psi_m(x,y)}{\Lambda_m(\omega^2 - \omega_m^2)} \int_0^L \sin(j\pi x'/L)$$
$$\times \psi_m(x',0) dx'. \tag{11}$$

Then, the total cavity pressure p_{cav} becomes

$$p_{\mathrm{cav}} = \sum_j u_j \cdot p_{\mathrm{cav},j}. \tag{12}$$

Similarly, the total external radiation p_{rad} is

$$p_{\mathrm{rad}} = \sum_i u_i \cdot p_{\mathrm{rad},j}. \tag{13}$$

Substitute Eqs. (12) and (13) into Eq. (4) and denote

$$Z_{\mathrm{cav},jl} = \int_0^L p_{\mathrm{cav},l}(x) \cdot \sin(j\pi x/L) dx \tag{14}$$

and

$$Z_{\mathrm{rad},jl} = \int_0^L p_{\mathrm{rad},l}(x) \cdot \sin(j\pi x/L) dx. \tag{15}$$

Thus, Eq. (4) is transformed to a truncated set of linear equations for the unknown coefficients u_j,

$$Z \cdot \{u_j\} + \frac{2}{\rho_0 c L} [Z_{\mathrm{rad},jl} - Z_{\mathrm{cav},jl}] \cdot \{u_j\} = \{I_j\}, \tag{16}$$

where

$$I_j = \frac{4}{\rho_0 c L} \int_0^L p_i \sin(j\pi x/L) dx. \tag{17}$$

Equation (16) can be solved via the inversion of matrix. In the actual calculation, modal truncation is needed. In Eq. (4), 400 TC modes are used to calculate the sound field in the trapezoidal cavity. For the duct acoustic modes $\varphi_n(x)$ in Eq. (8), the subscript n ranges from 0 to 50. The finite sine series

in Eq. (3) is truncated to $J = 80$. Numerical results show that the number of modes is normally enough as further increase in the number does not make significant difference for the purpose of this study.

With the matrix equation (16) solved, the averaged particle velocity over the MPP surface $\bar{u}(x)$ is obtained through the summation defined in Eq. (3). The total external pressure p_e is given as the sum of the blocked pressure $2p_i$ and the radiated pressure p_{rad},

$$p_e = 2p_i + p_{\mathrm{rad}}, \tag{18}$$

where p_{rad} is found with Eq. (8). Thus, the normal incidence sound absorption coefficient for the MPP absorber can be determined as

$$\alpha_N = \frac{\rho_0 c \int_0^L \mathrm{Re}[p_e^* \cdot \bar{u}(x)] dx}{|p_i|^2 L}, \tag{19}$$

where Re means the real part of a complex value and the asterisk denotes the complex conjugate. The surface impedance of the MPP absorber is given as

$$Z_s = \frac{p_e}{\bar{u}(x)}. \tag{20}$$

In the above modeling procedure, the sound wave p_i is assumed to be of normal incidence on the MPP surface. As a result, only normal incidence absorption coefficient α_N is predicted in Eq. (19), which can be conveniently measured using the impedance tube method. The overall modeling procedure, however, applies to situations of oblique incidence and random incidence. In the case of oblique incidence, the blocked pressure $2p_i$ in Eq. (2) becomes a function of the incidence angle, and the external radiation pressure p_{rad} changes accordingly. In the random sound field (diffuse field), sound waves impinge on the MPP at all angles, and the absorption coefficient can be determined as $\bar{\alpha} = \int_0^{\pi/2} \alpha_\theta \sin 2\theta d\theta$, where θ is the incident angle. In order to fully characterize the acoustic properties of the CBMPPA, sound absorption at oblique and random incidences is necessary, but this issue is left to future studies.

B. Model validation

The current theoretical model is first verified against a well-established method in literature where conventional MPP absorbers are involved, for instance, the equivalent electrical circuit method in (Maa, 1987, 1998). The MPP absorber considered here consists of a micro-perforated panel fitted in front of a solid wall with a constant air gap of $D = 0.06$ m. The properties of the MPP are $d = t = 0.2$ mm and $\sigma = 0.5\%$, where d is the orifice diameter, t is the panel thickness, and σ is the perforation ratio. The dashed curve in Fig. 3(a) shows the normal incidence absorption coefficients predicted by the equivalent electrical circuit method. Note that the predicted absorption curve has been shown to compare well with the measured results obtained with a standing wave tube (Maa, 1998). In order to predict the performance of the same MPP absorber using the present theoretical model, the constant air gap between the MPP and the solid wall is simulated as a rectangular cavity of the size 0.24×0.06 m^2, and

J. Acoust. Soc. Am., Vol. 127, No. 1, January 2010
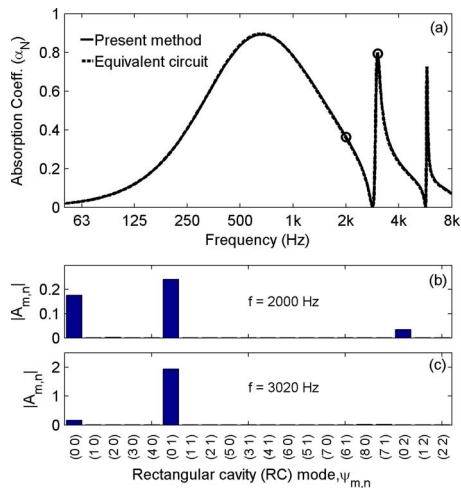
Wang *et al.*: Micro-perforated panel absorber   241

FIG. 3. (Color online) Predicted performance of a rectangular CBMPPA. The rectangular cavity is of the size 0.24×0.06 m². The properties of the MPP are $d=t=0.2$ mm and perforation ratio $\sigma=0.5\%$. (a) Comparison of the normal incidence absorption coefficients by the present model and the equivalent electrical circuit method in literature (Maa, 1998). (b) Amplitudes of the first 20 RC modes at frequencies $f=2000$ Hz. (c) Amplitudes of the first 20 RC modes at frequencies $f=3020$ Hz. The two frequencies are marked by open circles in (a) for easy identification.
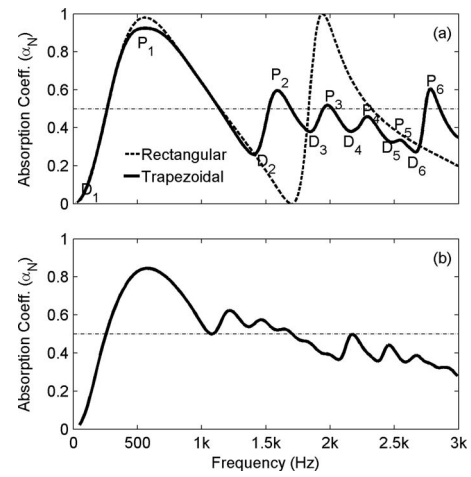

FIG. 4. Predicted absorption performance of the trapezoidal CBMPPAs. (a) Comparison between the trapezoidal CBMPPA (solid curve) and the rectangular CBMPPA of the same cavity volume. The configuration for the trapezoidal cavity is $L_a=0.4$ m, $L_b=0.06$ m, and $\gamma=11.3°$; the rectangular cavity is of the size $L_a=0.4$ m, $L_b=0.1$ m, and $\gamma=0$. (b) Absorption performance of the trapezoidal CBMPPA with a different configuration: $L_a=1$ m, $L_b=0.03$ m, and $\gamma=8.5°$. In both cases, the sound waves are incident on the MPP surface normally.

the infinite panel is reduced to a beam of finite length $L=0.24$ m. The simulated absorption coefficients with the present model are shown in Fig. 3(a) in solid curve. It can be seen that the predicted absorption curves by the two methods match with each other very well. Figures 3(b) and 3(c) show the amplitudes of the first 20 RC modal response at frequencies $f=2000$ and 3020 Hz, which are marked by open circles in Fig. 3(a) for reference. At $f=2000$ Hz, which lies in between the first and the second spectral peaks of the absorption curve, the (0,0) and (0,1) RC modes dominate the acoustic pressure inside the rectangular cavity. The (0,2) RC mode can also be observed, but its contribution is relatively small. At $f=3020$ Hz, which approximately corresponds to the second spectral peak of the absorption curve, only the (0,1) RC mode dominates. The (0,0), (0,1), and (0,2) RC modes correspond to the first three resonances of the infinite air gap in (Maa, 1987, 1998), indicating that the present model is consistent with the equivalent electrical circuit method. As mentioned in the Introduction, other cavity modes are almost not excited by the normal incident sound wave p_i since they are decoupled from the air motion in the micro-perforations.

III. NUMERICAL RESULTS

Based on the theoretical model developed in Sec. II, the normal incidence sound absorption properties of a MPP backed by a trapezoidal cavity are investigated numerically. The following set of parameters is used as the default values for the irregular-shaped CBMPPA:

$$d = 0.3 \text{ mm}, \quad t = 0.3 \text{ mm}, \quad \sigma = 1,$$

$$L_a = 0.4 \text{ m}, \quad L_b = 0.06 \text{ m}, \quad \gamma = 11.3°, \quad (21)$$

where d, t, and σ specify the properties of the perforated panel, and L_a, L_b, and γ define the geometrical configuration of the backing cavity. The choice of the default set of param-

eters in Eq. (21) is only to facilitate the analysis on the absorption mechanism of the irregular-shaped MPP absorber. No particular effort is made to seek optimal performance of the CBMPPA at the present stage.

A. Absorption performance

Figure 4(a) compares the absorption curves of the trapezoidal CBMPPA specified in Eq. (21) and a rectangular MPP absorber of the same cavity volume (i.e., $L_a=0.4$ m, $L_b=0.1$ m, and $\gamma=0$). The dashed curve shows the results for the rectangular absorber. Two spectral peaks can be observed within the frequency range of interest, and a dip occurs in between the two peaks, that is, around 1700 Hz. Since the absorption at the dip is negligible, it is the first peak that often determines the effective bandwidth for the conventional rectangular MPP absorber. The solid curve shows the absorption coefficients for the trapezoidal CBMPPA. In contrast with the two-peak spectrum for the rectangular MPP absorber, six distinct spectral dips (D₁–D₆) and peaks (P₁–P₆) are observed for the trapezoidal CBMPPA. The increased number of spectral peaks implies that more cavity modes are excited than in the case of the rectangular cavity. Around the first spectral peak P₁, the two absorbers demonstrate similar absorption performance. The second peak P₂ appears where the absorption performance of the conventional MPP absorber is very low, which makes it possible to achieve an absorber with wider effective bandwidth. The appearance of the following peaks P₃–P₆ maintains the absorption performance at a reasonably high level within the whole frequency range of interest. At the dips D₂–D₆, which roughly correspond to the resonances of the hard-walled trapezoidal cavity, a moderate sound absorption level is observed. This contrasts with the rectangular MPP absorber that has little absorption at the resonances of the backing cavity, as shown in Fig. 4(a) by the dashed curve at frequency f

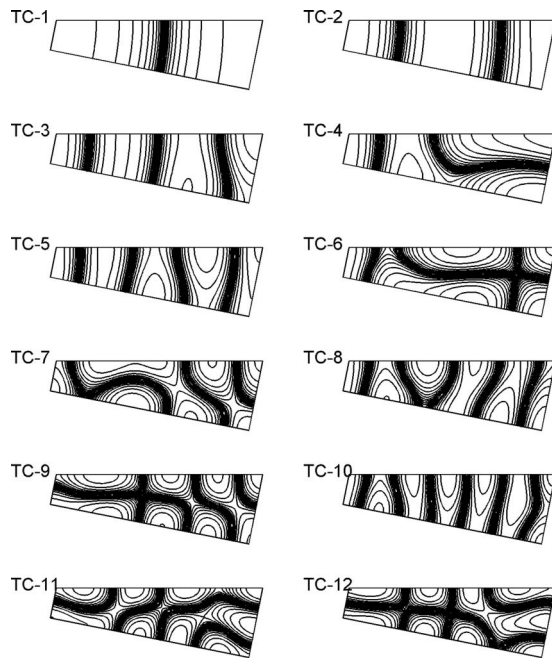Wang *et al.*: Micro-perforated panel absorber

FIG. 5. The spatial distribution of pressure of the first 12 non-zero TC modes of the default trapezoidal cavity. The sound pressure level difference between contours is 3 dB.
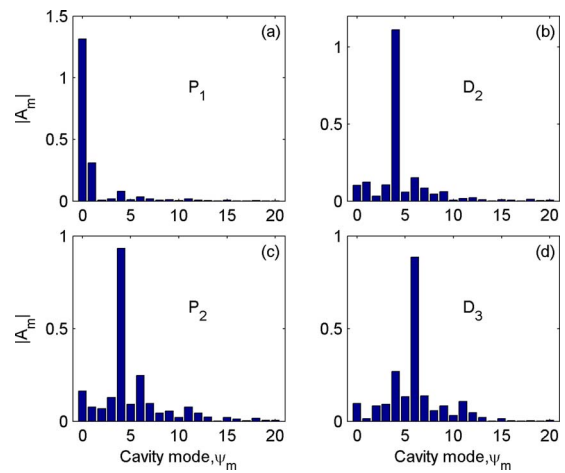

FIG. 6. (Color online) Amplitudes of the first 20 TC modes toward the total sound field in the backing cavity at the spectral peaks and dip frequencies. (a) The first peak, P_1. (b) The second dip, D_2. (c) The second peak, P_2. (d) The third peak, D_3.

=1700 Hz. It is worth noting that the occurrence of the peaks and dips can also be explained by the impedance matching conditions as in Maa (1998), but the impedance match only occurs in a local manner in the trapezoidal CBMPPA. An example of such local characteristics can be found in Fig. 7, in which the local impedance matching conditions for P_2 and D_2 are illustrated.

Note that the default set of parameters is not the optimum. A change in the geometrical configuration of the backing cavity can significantly alter the vibroacoustic coupling between the cavity and the MPP, and hence a better absorption performance might be achieved in terms of the effective bandwidth. Figure 4(b) shows the absorption curve for a different cavity configuration ($L_a=1$ m, $L_b=0.03$ m, and $\gamma =8.5°$) with the same MPP properties. The absorption coefficients at the first three dips in the curve are elevated to above half-absorption level, which gives rise to a wider absorption bandwidth. Therefore, a parametric study is necessary to systematically evaluate the effect of various design parameters on the absorption performance of the irregular-shaped CBMPPA, but this issue is left for future research.

Figure 5 depicts the first 12 nonzero modes of the trapezoidal cavity (TC modes) denoted as TC-1, TC-2,…, TC-12, respectively. It can be shown that these modes are evolved from individual or a family of RC modes of a corresponding rectangular cavity (Li and Cheng, 2004; Sum and Pan, 2006). The corresponding RC modes can be categorized into two types depending on whether the RC modes graze the inclined MPP or not. The TC modes TC-1, TC-2, TC-3, TC-5, TC-8, and TC-10 are evolved from the (1,0), (2,0), (3,0), (4,0), (5,0), and (6,0) RC modes, respectively. These RC modes graze the inclined MPP, and the evolved TC modes still nearly graze the inclined panel. The rest of the TC modes is evolved from RC modes that do not graze the inclined MPP. As more than one RC mode is involved significantly, the resulting TC mode has a relatively complicated mode shape. It is found that the two types of TC modes, i.e., the TC modes evolved from the grazing RC modes and those evolved from the nongrazing RC modes, contribute differently to the sound absorption of the trapezoidal MPP absorber.

The relationship between the free vibration characteristics of the trapezoidal cavity and the absorption performance of the trapezoidal CBMPPA is examined. Table I lists the resonance frequencies for the 12 TC modes shown in Fig. 5. It can be observed that the resonance frequencies for TC modes TC-4, TC-6, TC-7, TC-9, and TC-11 roughly coincide with the dips $D_2 - D_6$ in Fig. 4(a). The TC mode TC-12 also corresponds to a spectral dip but it is beyond the frequency range investigated. It can also be observed that all of these TC modes are evolved from nongrazing RC modes. Figure 6 illustrates the contributions of each TC mode toward the total sound field in the backing cavity at the selected spectral peaks and dip frequencies. At the peak P_1, the zero TC mode (which is not shown in Fig. 5) dominates over other cavity modes, as shown in Fig. 6(a). At the dip D_2 and the second peak P_2, the fourth TC mode plays a significant role in the total sound field, cf. Figs. 6(b) and 6(c). Such an observation can be repeated for all the other spectral peaks and dips. That

TABLE I. The first 12 resonant frequencies for the trapezoidal cavity.

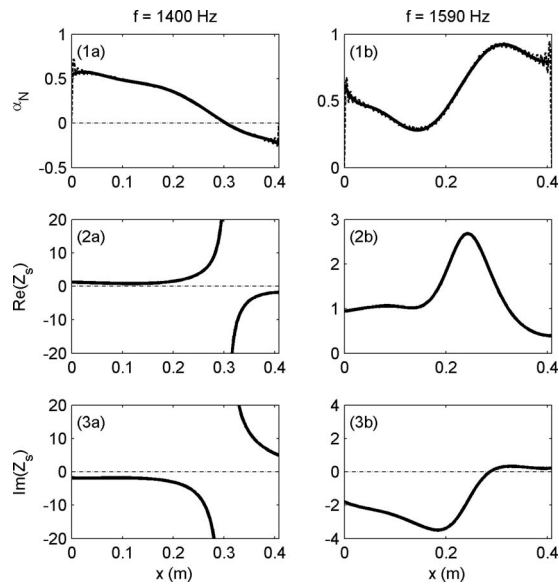| TC mode	1	2	3	4	5	6	7	8	9	10	11	12
Frequency (Hz)	437	857	1277	1385	1704	1793	2095	2143	2389	2556	2635	2677

FIG. 7. Local characteristics of absorption performance of the trapezoidal CBMPPA. The first row is for the absorption coefficients. The second and third rows are for the real part and the imaginary part of the surface impedance of the MPP absorber, respectively. Left column: $f=1400$ Hz; right column: $f=1590$ Hz.

is, the mode TC-6 dominates at D_3 and P_3, TC-7 dominates at D_4 and P_4, and so on. This feature is similar to that of a conventional MPP absorber with constant air gap. However, more cavity modes participate in the sound absorption process of the trapezoidal CBMPPA. Recall that only the RC modes such as (0,0), (0,1),(0,2),…, contribute to the sound absorption of the rectangular MPP absorber, as already shown in Fig. 3. For the trapezoidal cavity, all the TC modes evolving from non-grazing RC modes participate in the sound absorption of the MPP absorber. In other words, acoustic modes that are initially decoupled from the MPP in the rectangular configuration are now coupled with the air motion in the micro-perforations, and the coupling between the structure (MPP) and the enclosure (cavity) is greatly enhanced due to the inclination of the cavity wall.

B. Local sound absorption characteristics

Another distinct feature of the trapezoidal CBMMPA is its local distribution characteristics of the sound absorption coefficients across the micro-perforated surface. For the conventional MPP absorber with constant air gap, it is known that its absorption properties are the same over the whole micro-perforated surface as long as the perforation parameters are uniform. In the trapezoidal CBMPPA, the absorption properties vary across the micro-perforated panel even though the perforation parameters are the same. By removing the integration over L in Eq. (19), the distribution of the normal incidence absorption coefficients can be calculated as

$$\alpha_N(x) = \frac{\text{Re}[p_e^*(x) \cdot \bar{u}(x)]\rho_0 c}{|p_i|^2}. \tag{22}$$

Figures 7(1a) and 7(1b) show the distribution of the sound absorption coefficients at frequencies $f=1400$ and 1590 Hz, respectively. The two frequencies correspond to the dip D_2

and the peak P_2 shown in Fig. 4(a). The dashed lines are for the sound absorption coefficients calculated by Eq. (22) directly. Overshoots and small ripples exist in the absorption curves as the particle velocity $\bar{u}(x)$ is approximated with a finite series of sine waves, cf. Eq. (3). These artifacts are smoothed out in the least square sense so that the trend of variation will not be obscured, as shown by the solid lines in Figs. 7(1a) and 7(1b). It is worthy to note that the absorption coefficients become negative when $x>0.3$ m, which implies that some acoustic energy enters the trapezoidal cavity from other portion of the micro-perforated panel and is radiated out at the region $x>0.3$ m. That is to say that acoustic energy transfer may occur within the trapezoidal cavity. By the same token, the local absorption coefficients can be larger than unity at certain frequencies, though such a phenomenon is not demonstrated at the two particular frequencies.

The local absorption characteristics of the trapezoidal CBMPPA can be attributed to its varying impedance matching conditions between the MPP absorber and the incident sound field. The second and third rows of Fig. 7 show the real and imaginary parts of the surface impedance Z_s over the micro-perforated panel, respectively. For the trapezoidal CBMPPA, the real parts of the surface impedance manifest not only the resistance of the micro-perforated panel itself but also the effect of acoustic energy transfer within the trapezoidal cavity, which differs from the conventional MPP absorber with constant air gap. As a result, the real parts of the surface impedance Z_s is not distributed uniformly, and even negative values are observed under certain situations, cf. Fig. 7(2a). The imaginary part of the surface impedance Z_s characterizes the reactance of the MPP absorber, a small value of which usually means a good impedance matching between the absorber and the incident noise field. As shown in Fig. 7(3a), the local impedance mismatch at the region $x>0.25$ m explains the poor absorption performance at the same region in Fig. 7(1a). Likewise, the good impedance matching at $x>0.25$ m in Fig. 7(3b) accounts for the high absorption performance shown in Fig. 7(1b). As already shown in Fig. 6, the sound field inside the backing cavity is dominated by the cavity modes TC-4 for both $f=1400$ Hz (D_2) and $f=1590$ Hz (P_2). The region $x>0.25$ m roughly corresponds to the portion of the sound field in which the acoustic wave is perpendicular to the micro-perforated panel, which suggests the close relationship between the varying impedance conditions and the distorted TC modes.

IV. EXPERIMENTAL STUDY

The main objective of the experimental study is to validate the basic theoretical model established. To this end, the normal incidence sound absorption coefficients of a prototype CBMPPA are measured experimentally and compared with the theoretical predictions. The experimental rig is designed based on the two-microphone transfer-function method according to ISO-10534-2 (ISO, 1998), as shown in Fig. 8(a). The test rig consists of a straight rectangular duct (15-mm-thick acrylic) so that it can be considered to be acoustically rigid. A loudspeaker is connected at the left end as the excitation source. A prototype CBMPPA to be tested is
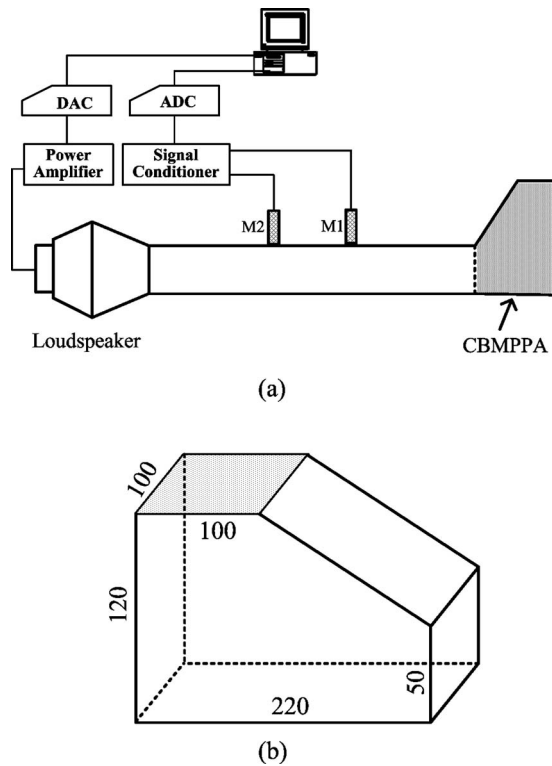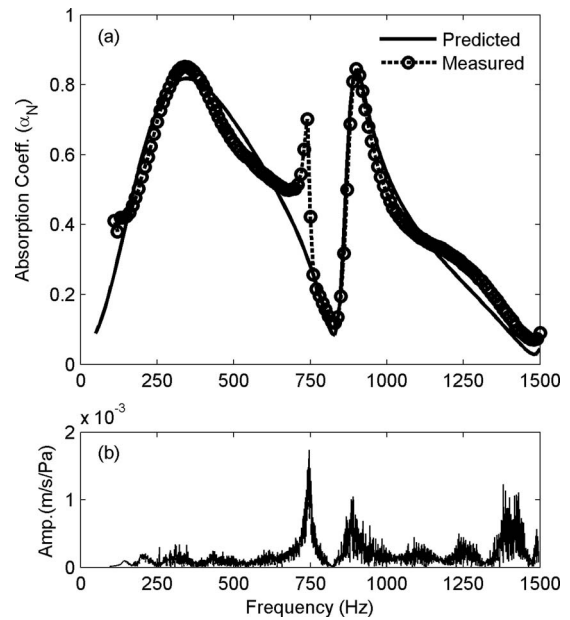
FIG. 9. Performance of the prototype CBMPPA. (a) Comparison between the measured and predicted sound absorption coefficients. (b) Amplitude of the measured frequency response of the MPP at (30 mm, 70 mm). The whole perforated area is of the size 100×100 mm². The reference sound pressure is measured about 3 mm in front of the panel in the duct.

FIG. 8. Schematic of the experimental rig. (a) The two-microphone measurement system. (b) Configuration of the prototype CBMPPA (dimensions in millimeters). The MPP of the size 100×100 mm² is located at the top surface.

installed at the other end of the duct. Two microphones M1 and M2 (B&K type 4187) measure the sound pressure inside the duct. The distance between the two microphones is properly selected according to the frequency range to be measured. From the transfer function between the two microphones, the surface impedance and the normal incidence absorption coefficient of the prototype CBMPPA can be determined. The cross section of the rectangular duct is of 100×100 mm². So, the first cut-on frequency in the rectangular duct is around 1700 Hz. Due to the limitation of the cross section of the test duct, it is hard to design a CBMPPA with the configuration shown in Fig. 2 to demonstrate the effect of the irregular-shaped cavity within the measurement frequency range of the test rig (say, lower than 1700 Hz). For this reason, the prototype CBMPPA has a configuration, as shown in Fig. 8(b). The cavity walls (other than the MPP) are also made of 15-mm-thick acrylic. The properties of the MPP [at the top surface in Fig. 8(b)] are

$$d = 0.415 \text{ mm}, \quad t = 0.46 \text{ mm}, \quad \sigma = 1.4, \tag{23}$$

where d is the orifice diameter, t is the thickness, and σ is the perforation ration in percentage. The MPP is made of aluminum. With the geometrical configurations shown in Fig. 8(b) and the MPP properties in Eq. (23), the absorption coefficients of the prototype CBMPPA are predicted using the theoretical model established in Sec. II.

Figure 9(a) compares the predicted and measured normal incidence absorption coefficients of the prototype CBMPPA. The solid curve shows the predicted results. Within the frequency range investigated, two peaks can be observed at frequencies $f = 350$ and 900 Hz, respectively. As analyzed in Sec. III, the occurrence of the second peak is attributed to the coupling between the MPP and the distorted cavity mode that are initially decoupled with each other in a rectangular configuration. Note that, for this particular design, the absorption performance at the "dip" frequency between the two peaks is not as good as that shown in Fig. 4, but it suffices to serve the objective of model validation. The dashed curve with open circles shows the measured absorption coefficients. As depicted in Fig. 9(a), the experimental result matches the theoretical predictions very well except that an extra absorption peak appears at $f = 740$ Hz. This extra peak is believed to be caused by the sound-induced panel vibration which is excluded in the current theoretical model. Figure 9(b) shows the amplitude of the measured frequency response of the MPP at the position (30 mm, 70 mm) with the reference sound pressure measured 3 mm in front of the panel in the duct. An obvious resonance peak can be observed at $f = 740$ Hz, indicating that strong panel vibration occurs. The corresponding deflection shape of the MPP is measured using a scanning vibrometer (PSV-400), and the panel vibration is found to be dominated by a strong volume-displacing vibration mode at this frequency. The possible mechanism involved for the effective sound absorption at this frequency might be the increased relative air particle velocity with respect to the panel vibration at the micro-perforations. Detailed discussion on the panel vibration effect can be found in Lee et al. (2005). As a summary, the experimental study demonstrates that the basic theoretical model of the irregular-shaped CBMPPA is correct. Sound-induced vibration of the panel itself may influence the absorption performance significantly and should be included in the theoretical modeling in future studies, especially when light material is used to fabricate the MPP.

J. Acoust. Soc. Am., Vol. 127, No. 1, January 2010

Wang et al.: Micro-perforated panel absorber   245

V. CONCLUSIONS

Owing to the altered vibro-acoustic coupling pattern, the sound absorption characteristics of a micro-perforated panel backed by an irregular-shaped cavity can be quite different from that of a conventional MPP absorber with constant air gap. From this observation, an irregular-shaped CBMPPA is proposed aiming for enhanced sound absorption performance. A 2D theoretical model is established by considering the full coupling among the MPP, the backing cavity, and the exterior sound field. Based on the verified theoretical model, the normal incidence absorption properties of a trapezoidal CBMPPA are investigated. The following conclusions can be drawn.

(1) The irregular-shaped backing cavity can significantly alter the sound absorption mechanisms and frequency distribution of overall sound absorption coefficients of the MPP absorber. Compared with the conventional MPP absorber with constant air gap, the irregular-shaped CBMPPA can produce more spectral peaks and achieve enhanced absorption performance at the troughs in the absorption curve. This property can be further explored to tune the effective absorption range of the CBMPPA by making appropriate changes to cavity shapes and dimensions. Meanwhile, it also suggests that the shape of the backing cavity could be used for future optimal design of the MPP absorber.

(2) Due to the inclination of the MPP, all TC modes that evolve from nongrazing RC modes are coupled to the air motion inside the micro-perforations, which accounts for the altered absorption pattern of the CBMPPA. Take the RC modes (m,n) of a 2D rectangular cavity for example. In a conventional MPP absorber with constant air gap, only the RC modes $(0,n)$ with $n=0,1,2,\ldots$, are coupled to the MPP. By replacing the rectangular cavity with a trapezoidal cavity, all TC modes evolving from both the RC modes $(0,n)$ with $n=0,1,2,\ldots$, and the RC modes (m,n), with m and $n>0$ are coupled to the MPP. The sound field at the spectral peaks and dips in the absorption curves are found to be dominated by a specific TC mode. The peak frequencies correspond to the resonant frequencies of the panel-cavity system, while the frequencies at the dips coincide roughly with the resonance frequencies of the rigid cavity alone.

(3) Unlike the uniform absorption performance over the MPP surface of the conventional MPP absorber, the irregular-shaped CBMPPA exhibits obvious local characteristics. Absorption coefficients less than zero and larger than unity can be observed at certain portion of the MPP surface due to the energy transfer within the backing cavity. The local absorption characteristics of the irregular-shaped CBMPPA are attributed to its varying impedance matching conditions, which in turn is closely related to the distorted acoustic mode shapes of the irregular-shaped cavity.

(4) The absorption coefficients of a prototype CBMPPA are measured using a standing wave tube and compared with the theoretical predictions. The experimental results are in good agreement with the theoretical predictions on the whole, demonstrating that the basic theoretical model is correct. Extra absorption peak is observed in the experiment, which is attributed to the sound-induced vibration of the MPP itself.

Asdrubali, F., and Pispola, G. (**2007**). "Properties of transparent sound absorbing panels for use in noise barriers," J. Acoust. Soc. Am. **121**, 214–221.

Atalla, N., and Sgard, F. (**2007**). "Modeling of perforated plates and screens using rigid frame porous models," J. Sound Vib. **303**, 195–208.

Bies, D., and Hansen, C. (**1996**). *Engineering Noise Control: Theory and Practice*, 2nd ed. (E&FN Spon, New York).

Cheng, L., Li, Y. Y., and Gao, J. X. (**2005**). "Energy transmission in a mechanically-linked double-wall structure coupled to an acoustic enclosure," J. Acoust. Soc. Am. **117**, 2742–2751.

Doak, P. E. (**1973**). "Excitation, transmission and radiation of sound from source distributions in hard-walled ducts of finite length. I. The effects of duct cross-section geometry and source distribution space-time pattern," J. Sound Vib. **31**, 1–72.

Droltleff, H., and Zhou, X. (**2001**). "Attractive room acoustic design for multi-purpose halls," Acta Acust. **87**, 500–504.

Fuchs, H. (**2001**). "Alternative fibreless absorbers—New tools and materials for noise control and acoustic comfort," Acta Acust. **87**, 414–422.

Fuchs, H. V., and Zha, X. (**1997**). "Acrylic-glass sound absorbers in the plenum of the Deutscher Bundestag," Appl. Acoust. **51**, 211–217.

ISO 10534-2 (**1998**). "Determination of sound absorption cefficient and impedance in impedance tubes," International Organisation for Standardization.

Kang, J., and Brocklesby, M. W. (**2005**). "Feasibility of applying microperforated absorbers in acoustic window system," Appl. Acoust. **66**, 669–689.

Kang, J., and Fuchs, H. V. (**1999**). "Predicting the absorption of open weave textiles and microperforated membranes backed by an air space," J. Sound Vib. **220**, 905–920.

Lee, D. H., and Kwon, Y. P. (**2004**). "Estimation of the absorption performance of multiple layer perforated panel systems by transfer matrix method," J. Sound Vib. **278**, 847–860.

Lee, Y. Y., Lee, E. W. M., and Ng, C. F. (**2005**). "Sound absorption of a finite flexible micro-perforated panel backed by an air cavity," J. Sound Vib. **287**, 227–243.

Li, Y. Y., and Cheng, L. (**2004**). "Modifications of acoustic modes and coupling due to a leaning wall in a rectangular cavity," J. Acoust. Soc. Am. **116**, 3312–3318.

Maa, D. Y. (**1975**). "Theory and design of microperforated-panel soundabsorbing construction," Sci. Sin. **18**, 55–71.

Maa, D. Y. (**1987**). "Microperforated panel wide-band absorber," Noise Control Eng. J. **29**, 77–84.

Maa, D. Y. (**1998**). "Potential of microperforated panel absorber," J. Acoust. Soc. Am. **104**, 2861–2866.

Meirovitch, L. (**2001**). *Fundamentals of Vibrations*, McGraw-Hill, Boston, MA.

Pan, J., Ming, R., and Guo, J. (**2004**). "Wave trapping barriers," in Proceedings of the Acoustics 2004, Gold Coast, Australia, pp. 283–287.

Putra, A. (**2007**). "Sound radiation from a perforated plate," ISVR Technical Memorandum No. 973, University of Southampton, UK.

Sum, K. S., and Pan, J. (**2006**). "Effects of the inclination of a rigid wall on the free vibration characteristics of acoustic modes in a trapezoidal cavity," J. Acoust. Soc. Am. **119**, 2201–2210.

Watts, G. (**1996**). "Acoustic performance of parallel traffic noise barrier," Appl. Acoust. **24**, 95–119.

Wu, M. Q. (**1997**). "Micro-perforated panels for duct silencing," Noise Control Eng. J. **45**, 69–77.